

1
2 **Permafrost changes in the northwestern Da Xing'anling**
3 **Mountains, Northeast China in the past decade**

4 Xiaoli Chang ^{1,2*}, Huijun Jin^{2,3*}, Ruixia He ², Yanlin Zhang ¹, Xiaoying Li ⁴, Xiaoying
5 Jin ² and Guoyu Li ²

6 ¹School of Earth Science and Spatial Information Engineering, Hunan University of Science and
7 Technology, Xiangtan, Hunan 411201, China,

8 ²State Key Laboratory of Frozen Soils Engineering, Northwest Institute of Eco-Environment and
9 Resources, Chinese Academy of Sciences, Lanzhou 730000, China,

10 ³School of Civil Engineering, Institute of Cold-Regions Science and Engineering, and Northeast-China
11 Observatory and Research-Station of Permafrost Geo-Environment (Ministry of Education), Northeast
12 Forestry University, Harbin 150040, China,

13 ⁴Key Laboratory of Sustainable Forest Ecosystem Management (Ministry of Education) and College of
14 Forestry, Northeast Forestry University, Harbin 150040, China

15 *These authors contributed equally to this work.

16 *Correspondence to:* R. He: ruixiahe@lzb.ac.cn

17
18 **Abstract.** Under a pronounced climate warming, permafrost has been degrading in most areas globally,
19 but it is still unclear in the northwestern part of the Da Xing'anling Mountains, Northeast China.
20 According to a ten-year observation of permafrost and active-layer temperatures, the multi-year average
21 of mean annual ground temperatures at 20 m was -2.83 , -0.94 , -0.80 , -0.70 , -0.60 and -0.49 °C,
22 respectively, at Boreholes Gen'he4 (GH4), Mangui3 (MG3), Mangui1 (MG1), Mangui2 (MG2),
23 Gen'he5 (GH5) and Yituli'he2 (YTLH2), with the depths of permafrost table varying from 1.1 to 7.0 m.
24 Ground cooling at shallow depths has been detected, resulting in declining thaw depths in Yituli'he
25 during 2009-2020, possibly due to relatively stable mean positive air temperature and declining snow
26 cover and dwindling local population. In most study areas (e.g., Mangui and Gen'he), permafrost
27 warming is particularly pronounced at larger depths (even at 80 m). These results can provide important
28 information for regional development and engineering design and maintenance, and also provide a long-
29 term ground temperature dataset for the validation of models relevant to the thermal dynamics of
30 permafrost in the Da Xing'anling Mountains. All of the datasets are published through the National
31 Tibetan Plateau Data Center (TPDC), and the link is <https://doi.org/10.11888/Geocry.tpdc.271752>
32 (Chang, 2021).

33 **1 Introduction**

34 Permafrost, defined as ground that remains at or below 0 °C consecutively for two or more years, is
35 widespread in high-latitude and high-elevation regions (Zhang et al., 2007). One quarter of the Northern
36 Hemisphere and 17% of the Earth's currently exposed land surface are underlain by permafrost (Gruber,
37 2012). Due to climate warming (Farquharson et al., 2019; Sim et al., 2021; Zhang et al., 2019; Ran et al.,
38 2018) and surface disturbances (Guo et al., 2018; Li et al., 2019; Li et al., 2021), permafrost has
39 experienced widespread degradation during the last decades (Jin et al., 2000; Jin et al., 2007; Zhang et
40 al., 2019; Jin et al., 2021; Chen et al., 2020), evidenced by deeper seasonal thawing (Luo et al., 2018),
41 thinning and warming permafrost (Gruber, 2012; Jin et al., 2021; Jin et al., 2007; Romanovsky et al.,
42 2010; Wu et al., 2022), and areal reduction (Li et al., 2021; Zhang et al., 2021). Permafrost change has
43 attracted extensive attention worldwide (Biskaborn et al., 2019), because it has significant potential
44 impacts on the terrestrial eco-hydrological processes (Zhang et al., 2017; Schuur and Mack, 2018; Zhang
45 et al., 2018a; Ala-Aho et al., 2021; Ran et al., 2022; Luo et al., 2022) and carbon cycling (Mu et al., 2020;
46 Schuur et al., 2015). In recent decades, huge efforts have been dedicated to developing physically based
47 models aiming to reproduce and predict the thermal dynamic processes of permafrost and their
48 consequences. However, lacking long term and systematic in-situ observation of permafrost temperature
49 becomes an apparent bottleneck for relevant analysis and model calibration or validation. Observations
50 in deep permafrost is especially rare and precious.

51 The areal extent of permafrost in China is estimated at about 1.59×10^6 km² (Ran et al., 2012), mainly in
52 the mountainous areas of northwestern China (Cao et al., 2018), on the Qinghai-Tibet Plateau (about
53 1.06×10^6 - 1.17×10^6 km²) (Zou et al., 2017; Cao et al., 2019), and in northeastern China (about 3.1×10^5
54 km²) (Zhang et al., 2021). The northern part of Northeast China, e.g., the Da Xing'anling Mountains, is
55 characterized by thick surficial deposit of organic soil and peat, dense vegetation, and widespread
56 distribution of wetlands in valley bottoms and lowlands, and extensive and stable inversion of air
57 temperature and snow cover in winter, resulting in strong regional differentiations in permafrost features
58 (Jin et al., 2007). Therefore, the permafrost in the Da Xing'anling Mountains is referred to as "Xing'an
59 (Hinggan)-Baikal permafrost (XBP)" (Jin et al., 2007), a distinct type of ecosystem-dominated
60 permafrost (Shur and Jorgenson, 2007). However, the intensity and progress of permafrost observation
61 in this region was falling far behind other permafrost regions in China, e.g., the Qinghai-Tibet Plateau

62 (Zhao et al., 2021; Wu et al., 2022). Most permafrost investigation and observation in Da Xing'anling
63 Mountains were aimed at serving some specific short-term projects in economic development,
64 engineering design and construction, e.g., road construction and coalmining (Jin et al., 2007), and they
65 were terminated upon the project completion without persistence. In recent years, numerous local studies
66 on permafrost change have been carried out. However, most of them were based on air and/or ground
67 surface temperatures provided by weather stations, reanalysis data (Wei et al., 2011; Zhang et al., 2018b;
68 Zhang et al., 2021), or short-term ground thermal observations (He et al., 2021; Jin et al., 2007). Without
69 direct observation of ground temperature profiles and their temporal changes, it is hard to more accurately
70 feature and evaluate the latest distribution and future changes of permafrost in Northeast China under the
71 combined influences of warming climate and human activities (Serban et al., 2021). Similar to the
72 Circumpolar Active Layer Monitoring (CALM) sites (Brown et al., 2000; Grebenets et al., 2021;
73 Shiklomanov et al., 2012), or CALM-South sites (Guglielmin, 2006; Guglielmin et al., 2012; Hrbáček et
74 al., 2021), a comprehensive and persistent observing system was gradually established since 2009 at
75 Gen'he (GH), Yituli'he (YTLH), and Mangui (MG) in the northwestern part of the Da Xing'anling
76 Mountains, Northeast China. Periodical collection and calibration of data on the thermal regimes of soils
77 in the active layer and permafrost at depths have been carried out in boreholes, generally reaching 20 m
78 in depth and one of them, 80 m. Thus, the observing system presents an opportunity to investigate the
79 thermal characteristics of XBP at depths and to understand and evaluate the temporal changes in
80 permafrost features in different landscapes under a warming climate. It can obtain a long-term ground
81 temperature dataset for calibration and validation of models relevant to the thermal dynamics of
82 permafrost in the Da Xing'anling Mountains, and provide important information for regional planning,
83 development, and engineering design and maintenance in Northeast China.

84 **2 Study area**

85 The Gen'he Station of China Forest Ecological Research Network (CFERN), Yituli'he Permafrost
86 Observatory (YTLH), and Mangui Permafrost Station (MG) are found in the discontinuous permafrost
87 zone of Northeast China (Figure 1), where it is characterized by a cold temperate continental climate
88 under the influences of alternating monsoons. The multi-year average of mean annual air temperature
89 (MAAT) was -4.0 °C at Gen'he (1961–2020), -5.2 °C at Yituli'he (1965–2005), and -5.8 °C at Mangui

90 (1996–2005). During the same periods, the multi-year average of annual precipitation was 440 mm at
91 Gen’he, 460 mm at Yituli’he, and 480 mm at Gangui (Yang, 2007; Jin et al., 2007). The precipitation
92 falls mainly in the form of summer rain, and snowfall accounts for about 12~20% (in snow water
93 equivalent, or SWE). Stable snow cover on the ground surface usually starts to occur in the late October
94 and generally disappears in the next April.

95 In the vicinity of CFERN, five boreholes were installed at Gen’he, and the datasets at GH4 and GH5
96 (Figure 1) with good quality were presented in this study. Two boreholes (YTLH1 and YTLH2) and three
97 boreholes (MG1, MG2 and MG3) were installed at YTLH and MG, respectively (Figure 1). The
98 vegetation differs slightly from site to site at all mentioned boreholes (Table 1). For example, GH4 is
99 located in a larch (*Larix gmelinii*) forest, whereas GH5, YTLH1, YTLH2 and MG2 are in sedge (*Carex*
100 *tato*) meadows. MG3 is in an open backyard, and MG1 is located in a birch (*Betula*) shrubland with
101 sedges (*Carex tato*) as an understory. The soil types at all boreholes are the same, i.e., brown coniferous
102 forest soil.

103 Among the seven boreholes, YTLH1 with a depth of 8.15 m was first installed for monitoring the
104 hydrothermal dynamics of active layer and shallow permafrost at the end of 2008, with weekly manual
105 measurement of soil temperatures since 2009. However, in order to monitor the permafrost temperature
106 at the depth of zero annual amplitude (generally at 10-25 m in Northeast China), YTLH2 was drilled to
107 a depth of 20 m at a nearby site (10 m away from the YTLH1) with almost identical physical and
108 vegetative conditions on the ground surface. Thermistor cables for monitoring the ground temperatures
109 were permanently installed in the boreholes since 2010. GH4, GH5, MG1, MG2 and MG3 have been
110 installed and started working since the beginning of 2012, but with different observational frequencies
111 (Table 1). All the thermistor cables were assembled with same technology standards by the State Key
112 Laboratory of Frozen Soils Engineering (SKLFSE) in Cold and Arid Regions Environmental and
113 Engineering Research Institute (CAREERI; now renamed to the Northwest Institute of Eco-Environment
114 and Resources, or NIEER) of CAS (Chinese Academy of Sciences). The accuracy of ground temperature
115 measurement is ± 0.05 °C in the temperature range from -30 to $+30$ °C, and ± 0.1 °C in ranges from -45
116 to -30 °C and from $+30$ to $+50$ °C.

117 For continuous observation, the thermistor cables at GH4 were connected to a Micrologger of CR3000
118 (USA), and the ground temperatures were automatically collected in an hourly time step, whereas the
119 ground temperatures at other boreholes were manually measured with a multi-meter (Fluke 189®).

120 Unfortunately, not all records for ground temperatures are complete in time for all boreholes. For example,
121 there were two hiatuses for the records of GH4 (2014-2016 and 2017-2019) due to the logger damage.
122 Manual records from January to June in 2014 for other boreholes were lost in mailing. The measurement
123 at MG3 was halted in 2016 because of borehole damage and that at GH5 and YTLH2, in 2020, due to
124 the outbreak of the COVID-19 virus and the ensued traffic control. The specifics are presented in Table
125 1.

126 **3 Results**

127 **3.1 Ground temperatures in near-surface permafrost and active layer**

128 Ground temperatures of near-surface soil (e.g., at depths of 1 and 2 m) responds quickly to changes in
129 air temperature, but the change patterns of ground temperatures show a reduction of amplitude with
130 increasing depth in all boreholes. In boreholes GH4, MG3, YTLH1 and YTLH2, seasonal variations in
131 ground temperature still could be detected at the depth of 5 m. However, at depths of 3 and 4 m, variations
132 in winter ground temperatures gradually flattens out in boreholes GH5, MG1 and MG2, and only the
133 annual variability in summer ground temperatures can be detected at the depth of 5 m (Figure 2).
134 Therefore, only a small temperature amplitude (0.5~1.0°C) was detected at the depth of 5 m in
135 comparison with that at 3 m (2~3°C).

136 Based on the thermal observation at MG1, 2.6 m (2017) and 1.9 m (2020) in depth were respectively the
137 maximum and minimum depths of permafrost table (Table 2). Combining the data in Figure 2b and other
138 observational data, the active layer thickness (ALT) at MG2 increased from 4.3 m (2012) to 4.8 m (2016),
139 but thinned to 4.2 m (2019) afterwards. The permafrost table at MG3 was located at 2.8 m (2012 and
140 2013), 4.0 m (2014) and 3.3 m (2015) in depth during the observation period. Subtle freeze-thaw cycles
141 were observed at 2.0 m in depth in GH4 (Figure 2a₂), and the 0 °C isotherms in Figure 3a indicated a
142 range of ALT from 2.2 m (2016) to 2.0 m (2018). In GH5, there still exist obvious freeze-thaw cycles at
143 the depth of 6.0 m, despite with a small varying range in ground temperature (0.5°C). However, the
144 ground temperature at the depth of 7.0 m stayed constantly below 0 °C all year round during the
145 monitoring period, approximating to 0 °C and with a multi-year average of mean annual ground
146 temperature at -0.08°C. That is, the thawing front reached down to the depth of 7.0 m every year (Figure
147 3b), which means the permafrost table here has been lowered to 7.0 m in depth. In YTLH1, ground

148 thawing occurred occasionally at 2.0 m, for an example, in October 2016, but the ALT mostly varied
149 from 1.5 m (2011) to 1.0 m (2017) during the observation (Figure 3c). In the same period in 2016, $-0.1\text{ }^{\circ}\text{C}$
150 was registered as the highest temperature at 2.0 m in depth in YTLH2 (Figure 2c₂), but an above-zero
151 temperature at 1.5 m depth. The depth of permafrost table fluctuated between 1.6 m (2017) and 2.0 m
152 (2011 and 2016) (Figure 3d and Table 2).

153 **3.2 Changes of permafrost temperature at depth**

154 Figure 4 highlights the changes in thermal regimes of permafrost at different depths in boreholes MG1,
155 MG2 and MG3. Ground temperature was on the rise, but its amplitude decreased with depth since the
156 beginning of observation in 2012. The depth of zero annual amplitude (ZAA) was estimated to be the
157 place where ground temperature changes by no more than $0.1\text{ }^{\circ}\text{C}$ throughout a year (Everdingen, 1998
158 (revised 2005)). Although the ground temperature was not measured periodically with a very fine time
159 step and some values were lost, the estimation could still be reasonable, because the temperature
160 fluctuation in deep ground is significantly dampened. According to the monitoring data, the depth of
161 ZAA varies among different boreholes (Table 2) without considering interannual changes. In order to
162 show more accurate thermal states of permafrost, ground temperatures of 20 m were chosen to compare
163 within different boreholes in this study. In MG1, the varying amplitudes of ground temperatures for
164 depths deeper than 8 m were no more than $0.4\text{ }^{\circ}\text{C}$, and seasonal variability was hardly detectable at depths
165 of 16 and 20 m. The results of linear fitting (red trend lines) indicate an overall warming trend of
166 permafrost during 2012-2020. A multi-year average of mean annual ground temperature (MAGT, at 20
167 m; from 2012 to 2020) of $-0.77\text{ }^{\circ}\text{C}$ was obtained in borehole MG1. In MG2, the ground temperature
168 varied slightly ($\pm 0.06\text{ }^{\circ}\text{C}$) with the seasons even at the depth of 20 m, where the MAGT was about
169 $-0.69\text{ }^{\circ}\text{C}$. Permafrost here was also warming, with a rising amplitude of $0.1\sim 0.2\text{ }^{\circ}\text{C}$ from 2012 to 2020.
170 The valid monitoring period was less than 5 years in MG3 (1 January 2012 to 29 April 2016), when the
171 largest ground temperature range of $0.2\text{-}0.5\text{ }^{\circ}\text{C}$ was detected between the depths from 8 to 20 m. Similar
172 to that in MG2, the permafrost temperature at the depth of 20 m in borehole MG3 has been experiencing
173 some seasonal variations, with a multi-year average of MAGT at $-0.94\text{ }^{\circ}\text{C}$ (Table 2).
174 During 2012-2020, permafrost at depths of 8 and 20 m in GH4 and GH5 (Figure 5) warmed by $1.5\text{-}0.2$
175 and $0.2\text{-}0.1\text{ }^{\circ}\text{C}$, respectively. The warming of permafrost at GH5 was insignificant in comparison with
176 that at other sites. Mean annual ground temperature at 8 m in depth have slightly warmed from $-0.17\text{ }^{\circ}\text{C}$

177 in 2012 to $-0.16\text{ }^{\circ}\text{C}$ in 2019, and; the MAGT at 20 m in depth, from -0.60 to $-0.57\text{ }^{\circ}\text{C}$ over the same
178 period. MAGT at 20 m in depth was averaged at $-0.59\text{ }^{\circ}\text{C}$ during 2012-2019. However, permafrost at
179 GH4 was obviously colder, with a multi-year average of MAGT at $-2.84\text{ }^{\circ}\text{C}$ at 20 m in depth. According
180 to Figure 5, ground temperatures at depths of 8-20 m fluctuated seasonally. However, seasonal variations
181 in ground temperature dwindled gradually at depths deeper than 30 m (Figure 6), leaving only inter-
182 annual variations. Ground temperatures in GH4 increased with increasing depth (-2.51 , -1.76 and
183 $-0.41\text{ }^{\circ}\text{C}$ at 30, 50 and 80 m, respectively), whereas the thermal fluctuations declined downwards ($0.2\text{ }^{\circ}\text{C}$
184 at 20 and 30 m in depth, but $0.03\text{ }^{\circ}\text{C}$ at 80 m). During 2012-2020, the permafrost at depths of 30-80 m at
185 GH4 was warming at an average rate of $0.04\text{-}0.20\text{ }^{\circ}\text{C}/\text{dec}$.

186 In Borehole YTLH2, remarkable seasonal variations were noted at each measured depth. The seasonal
187 amplitude of ground temperature gradually dampened with increasing depth, varying from approximately
188 $0.5\text{ }^{\circ}\text{C}$ at 8 m in depth to less than $0.1\text{ }^{\circ}\text{C}$ at 20 m. Unlike permafrost in Mangui town and Gen'he city, a
189 significant cooling of permafrost was detected at all depths except 20 m at YTLH2 during the 10-year
190 observation (Figure 7). The average rate of temperature change at 20 m depth is close to $0\text{ }^{\circ}\text{C}/\text{dec}$ and
191 the MAGT here has been roughly maintained at $-0.49\text{ }^{\circ}\text{C}$ in the past decade (Table 2).

192 **4 Discussion**

193 **4.1 Changes of near-surface permafrost temperatures**

194 Based on the analysis in Section 3.1, it can be inferred that changes in ground thermal regimes (especially
195 in ALT) of the ecosystem-dominated permafrost on the northwestern slope of Da Xing'anling Mountains
196 are mainly controlled by the changes in local factors, such as vegetation and snow covers and human
197 activities. For example, ALT ranges from 2.5 m in 2016 and 2017 to 1.9 m in 2020 for the borehole in
198 shrubs (MG1), 4.8 m in 2017 to 4.2 m in 2020 for the borehole in sedge meadow (MG2), and 2.9 m in
199 2012 to 4.0 m in 2014 for the borehole in a farmer's backyard (MG3) during the observation period.
200 Apparently, the borehole MG1, far away from downtown Mangui, had the least ALT because of more
201 shading effect of shrubs than that of meadow (MG2) and less anthropogenic impact than that of backyard
202 (MG3). A declining trend of ALT was also observed in the Nanwenghe Wetlands Reserve on the southern
203 slope of the Da Xing'aning-Yile'huli Mountain Knots, Northeast China, probably driven by a rising
204 surface and thermal offsets of vegetation cover and organic soils (He et al., 2021). Additionally, at MG3,

205 the smaller ALT could be attributed to the shading effect of the farmer's house and more heat loss to the
206 atmosphere caused by snow removal in the yard in winter as well. In Gen'he, at the site of GH4 in a
207 primeval forest, ALT remained unchanged at 2.2 m from 2012 to 2016 and, without human disturbance,
208 permafrost was well-preserved. On the contrary, at the GH5 site in the suburb meadow frequently
209 disturbed by the nearby livestock, a complex thermal regime was observed in the active layer. Ground
210 temperatures at the depths of 3.5-6.0 m were below 0° C from March to September and above 0° C in
211 other time every year, and; not until 7.0 m in depth, where it became below 0° C all the year round. By
212 definition, the active layer is the layer above permafrost that freezes in winter and thaws in summer.
213 Therefore, 7 m is supposed to be the reasonable ALT or the depth of permafrost table, and there might
214 be no supra-permafrost subaerial talik (Jin et al., 2021) between the active layer and the permafrost table
215 at this site, i.e., attached permafrost. However, the supra-permafrost subaerial talik, which has appeared
216 in the Nanwenghe Wetlands Reserve about 300 km to the east of the study site (He et al., 2021), may
217 develop at this site in future. In Yituli'he, the two boreholes (YTLH1 and YTLH2) are, about 20 m apart,
218 both in the meadowy swamp to the east of the railway and to the west of highway. Permafrost here is
219 well developed, partially attributed to the sufficient moisture provided by lowland swamp, which also
220 possibly facilitates the formation of ice wedges (Yang and Jin, 2011).

221 Notably, there was a decreasing trend in ground temperatures at shallow depths no matter in summer or
222 winter during 2010-2020 (Figure 2), suggesting a cooling permafrost at shallow depths in the last decade
223 on the northwestern slope of the Da Xing'anling Mountains. The maximum thaw depth (MTD) in
224 Yituli'he rose gradually with fluctuations during 1980-2005, and it showed a downward trend during
225 2010-2019 (Figure 8). This could be related to the thriving vegetation, and declining winter precipitation
226 or snow cover in this area during the observational period. In the last decade, although the mean positive
227 air temperature (MPAT) barely changed in Gen'he (Fig 9b), precipitation in warm seasons increased
228 slightly, leading to a wetter condition in favor of vegetation thriving. For example, the maximum
229 vegetation height of *Carex tato* at YTLH1 and YTLH2 grew significantly from 2009 to 2014. Bushes
230 have also emerged recently near the borehole. Thriving vegetation reduces the solar irradiance incident
231 onto the soil surface in summer, cooling the ground. On the contrary, the winter precipitation (Figure 9a)
232 and snow cover, including the maximal snow depth (Figure 9c) and snow duration (Figure 9d), declined
233 slightly. The thermal insulation effect of snow cover weakens when the depth of snow cover declines,
234 which will lead to a larger heat removal from the permafrost to air in winter and drive the permafrost

235 cooling. Detailed mechanisms for the cooling permafrost will be further investigated with the help of
236 some physically based models after complementing observations on the interactions of energy balance
237 between the permafrost, vegetation, and snow cover.

238 **4.2 Changes of permafrost temperatures at depth**

239 **Permafrost in Mangui**

240 During the observation period, the averages of MAGTs at the depth of 20 m were -0.79 , -0.70 and -0.93
241 $^{\circ}\text{C}$, respectively, in shrubs (MG1), meadow (MG2) and the farmer's backyard (MG3), indicating a poor
242 correlation between the thermal state of deep permafrost and vegetation cover or anthropic disturbances.
243 However, there was a close relationship between the permafrost change at depth and land surface
244 conditions. The permafrost deeper than 8 m was significantly warming in the last decade under a warming
245 climate (Figure 4). In MG1 and MG2 in particular, the rates of ground warming increased slightly with
246 depth (<0.3 $^{\circ}\text{C}/\text{dec}$ for MG1 and <0.2 $^{\circ}\text{C}/\text{dec}$ for MG2). Within the zone of discontinuous permafrost,
247 the negative relationship between effective leaf area index (LAI_e) and soil moisture content may
248 contribute to differential rates of permafrost thaw (Baltzer et al., 2014). Therefore, more effective water
249 uptake by shrubs than meadow results in lower soil moisture, leading to a more rapid thaw of permafrost
250 at MG1 than that at MG2. The warming rate of permafrost in MG3, with a large warming range,
251 decreased with depth (0.5 $^{\circ}\text{C}/\text{dec}$ at depths of 10 and 12 m, but approximately 0.2 $^{\circ}\text{C}/\text{dec}$ at depths of 16
252 and 20 m), probably due to short monitoring period and less data. However, it does verify that, in Mangui,
253 permafrost at depth is warming or degrading in the last decade.

254 **Permafrost in Gen'he**

255 Indeed, there exists some long periods with missing data at GH4. However, although the fluctuation of
256 ground temperatures is relatively large at surface layers, the collected data have generally captured the
257 maximal and minimal ground temperature for some important years. Simply by a visual inspection, the
258 minimal or maximal ground temperatures in the observed years has an apparent warming trend from
259 2012 to 2020, which has a good coincidence with the trend analysis in this study. That is, although the
260 missing values could make some loss for the accuracy of trending analysis, or make it less robust, they
261 will not change the trend in an antipodal way. In addition, in the ground deeper than 8 m, the annual
262 fluctuation of ground temperature was much less than that in the surface layers, as shown in Figures 5
263 and 6. The missing values will not vary too much from the closest collected values in time. Therefore,

264 we assume that the influence of missing values on the trending analysis of ground temperature at depth
265 will be smaller than that in the surface layers, and it will decrease with depth, which can be inferred from
266 Figures 5 and 6.

267 In GH4, lower ground temperatures and greater warming rates were observed in comparison with those
268 in GH5 in the last decade (Figure 5). Even at the depths of 70 and 80 m, the ground temperatures were
269 still rising with time at appreciable warming rates (Figure 6). A subtle warming trend of permafrost at
270 depths of 8-20 m in GH5 was also detected with a rate of 0.04 °C/dec during the observation period
271 (Figure 5). This warming rate of ground temperature is similar to that of the Borehole 85-8A in the
272 southern zone of discontinuous permafrost in North America, where the permafrost is often vertically in
273 isothermal condition and close to 0 °C in ground temperature (Smith et al., 2010). In this situation, latent
274 heat effects are considered as the key factor for leading to isothermal conditions in the ground and
275 allowing permafrost to persist under a warming climate (Smith et al., 2010). If the effect of large thermal
276 inertia lasts long enough, the supra-permafrost subaerial talik will be highly likely to form and permafrost
277 will be gradually buried. Overall, the permafrost at depth in forested landscape in Gen'he is in an evident
278 warming trend at present.

279 **Permafrost in Yituli'he**

280 According to a previous study (Jin et al., 2007), MAGT at 13 m in Yituli'he rose by 0.2 °C during 1984-
281 1997, continuously rising from -1.00 °C in 1997 to -0.55 °C in 2010, except during the short suspension
282 of monitoring (2005-2008), and peaking at -0.53 °C in 2013. After that, it kept lowering consecutively
283 and by 2018 it was lower than -0.70 °C, showing an evident cooling trend of permafrost in a sharp
284 contrast to the ground warming trends in Gen'he, Mangui, and other permafrost regions in the world
285 (Douglas et al., 2021; Farquharson et al., 2019). Based on an investigation, there was once a Railway
286 Branch Administration in Yituli'he town since 1964s to 1970s, with a population of over 30,000, but the
287 branch was terminated in 1998. After that, more and more people emigrated and less than 10,000
288 residents have remained at present, thus leaving a chance for recovery of the local eco-environment and
289 permafrost temperature.

290 So far, the mitigation of permafrost degradation becomes considerably difficult in the context of a
291 persistent climate warming (Brown et al., 2015; Luo et al., 2018). However, within the dried margin of
292 the Twelvemile Lake (66°27'N, 145°34'W), permafrost aggradation has taken place due to willow shrub

293 uptake of summer recharge and summer shading recharge reduction (Briggs et al., 2014). Beer et al.
294 (Beer et al., 2020) also found that most permafrost-affected soil could be preserved by increasing the
295 population density of big herbivores in northern high-latitude ecosystems as a result of reducing
296 insulation of winter snow cover. The fact that permafrost is cooling in Yituli'he demonstrates that the
297 ecosystem-protected permafrost in discontinuous permafrost zone may recover if the disturbances, such
298 as human activities, dwindle. Thus, our research results would provide key evidence for the preservation
299 of permafrost in areas with intense past anthropic disturbances (Serban et al., 2021).

300 **5 Conclusions**

301 Long-term records of permafrost monitoring presented here from the northwestern flank of the Da
302 Xing'anling Mountains in Northeast China show some important characteristics of ground thermal
303 regimes in the past eight years (2012-2020). The lowest MAGT at 20 m in depth was -2.83 °C in GH4
304 in a primeval larch forest, and -0.94 , -0.80 , -0.70 , -0.60 and -0.49 °C, respectively, at MG3, MG1,
305 MG2, GH5 and YTLH2. The maximum of burial depth of permafrost table at about 7.0 m was discovered
306 in GH5, and the minimum, 1.1 ~ 1.5 m at YTLH1. The permafrost table was at depths of about 2.0 m at
307 GH4 and YTLH2, and 2.5, 5.0 and 4.0 m at MG1, MG2 and MG3, respectively. Local factors, such as
308 vegetation and snow cover and human activities, are supposed to be mainly responsible for the changes
309 in ALT and thermal state of shallow permafrost in the study area. The most important fact is that ground
310 cooling at shallow depths, as well as the declining ALT in Yituli'he after 2009, has been detected during
311 the observation period, which is probably caused by fairly constant MPAT (mean positive air temperature)
312 and weakened insulation of winter snow cover.

313 Apart from Yituli'he, permafrost warming at depth was particularly pronounced during the observation
314 period, even at depths of 70 and 80 m, with different ground warming rates. It is noteworthy that the
315 geothermal gradient at depth in GH5 is almost zero (vertically no change) and with MAGT at about 0 °C
316 due to huge thermal inertia of the ice-rich permafrost. This may most likely lead to the formation of
317 supra-permafrost subaerial talik soon. At the Yituli'he Permafrost Observatory, permafrost has been
318 cooling since the re-establishment of monitoring program in 2010; the rapidly declining local population
319 might have relieved its stress on the eco-environment and resulted in permafrost recovery. This fact
320 makes it possible to mitigate the permafrost degradation in zones of ecosystem-dominated permafrost,

321 offering a new thought for permafrost protection.

322 **Author Contributions**

323 XC, HJ, and RH designed the study. XC wrote the manuscript and performed the analysis. YZ
324 plotted the figures. XL, XJ and GL contributed parts of the field data. HJ improved the writing and
325 structure of the paper.

326 **Competing interests**

327 The contact author has declared that neither they nor their co-authors have any competing interests.

328 **Disclaimer**

329 Publisher's note: Copernicus Publications remains neutral with regard to jurisdictional claims in
330 published maps and institutional affiliations.

331 **Special issue statement**

332 This article is part of the special issue "Extreme Environment Datasets for the Three Poles". It is
333 not associated with a conference.

334 **Acknowledgements**

335 Thanks go to the Inner Mongolia Agricultural University for fieldwork support and the Gen'he Weather
336 Bureau for meteorological data provision. This study was financially supported by the National Natural
337 Science Foundation of China (Grant Nos. 41971079, 41671059, 41871052 and U20A2082) and the
338 Natural Science Program of Hunan Province (Grant No. 2020JJ5161).

339 **Data availability**

340 The dataset is available from the National Tibetan Plateau/Third Pole Environment Data Center
341 (<https://doi.org/10.11888/Geocry.tpdc.271752>, Chang X, 2021).

342 **Reference**

343 Ala-Aho, P., Autio, A., Bhattacharjee, J., Isokangas, E., Kujala, K., Marttila, H., Menberu, M., Meriö, L.
344 J., Postila, H., Rauhala, A., Ronkanen, A. K., Rossi, P. M., Saari, M., Haghghi, A. T., and Kløve, B.:
345 What conditions favor the influence of seasonally frozen ground on hydrological partitioning? A
346 systematic review, *Environmental Research Letters*, 16, 043008, 10.1088/1748-9326/abe82c, 2021.
347 Baltzer, J. L., Veness, T., Chasmer, L. E., Sniderhan, A. E., and Quinton, W. L.: Forests on thawing
348 permafrost: fragmentation, edge effects, and net forest loss, *Global change biology*, 20, 824-834,

349 10.1111/gcb.12349, 2014.

350 Beer, C., Zimov, N., Olofsson, J., Porada, P., and Zimov, S.: Protection of Permafrost Soils from Thawing
351 by Increasing Herbivore Density, *Scientific reports*, 10, 4170, 10.1038/s41598-020-60938-y, 2020.

352 Biskaborn, B. K., Smith, S. L., Noetzli, J., Matthes, H., Vieira, G., Streletskiy, D. A., Schoeneich, P.,
353 Romanovsky, V. E., Lewkowicz, A. G., Abramov, A., Allard, M., Boike, J., Cable, W. L., Christiansen,
354 H. H., Delaloye, R., Diekmann, B., Drozdov, D., Etzelmüller, B., Grosse, G., Guglielmin, M., Ingeman-
355 Nielsen, T., Isaksen, K., Ishikawa, M., Johansson, M., Johannsson, H., Joo, A., Kaverin, D., Kholodov,
356 A., Konstantinov, P., Kröger, T., Lambiel, C., Lanckman, J.-P., Luo, D., Malkova, G., Meiklejohn, I.,
357 Moskalenko, N., Oliva, M., Phillips, M., Ramos, M., Sannel, A. B. K., Sergeev, D., Seybold, C., Skryabin,
358 P., Vasiliev, A., Wu, Q., Yoshikawa, K., Zheleznyak, M., and Lantuit, H.: Permafrost is warming at a
359 global scale, *Nature Communications*, 10, 264, 10.1038/s41467-018-08240-4, 2019.

360 Briggs, M. A., Walvoord, M. A., McKenzie, J. M., Voss, C. I., Day-Lewis, F. D., and Lane, J. W.: New
361 permafrost is forming around shrinking Arctic lakes, but will it last?, *Geophysical Research Letters*, 41,
362 1585-1592, <https://doi.org/10.1002/2014GL059251>, 2014.

363 Brown, D. R. N., Jorgenson, M. T., Douglas, T. A., Romanovsky, V. E., Kielland, K., Hiemstra, C.,
364 Euskirchen, E. S., and Ruess, R. W.: Interactive effects of wildfire and climate on permafrost degradation
365 in Alaskan lowland forests, *Journal of Geophysical Research: Biogeosciences*, 120, 1619-1637,
366 <https://doi.org/10.1002/2015JG003033>, 2015.

367 Brown, J., Hinkel, K. M., and Nelson, F. E.: The circumpolar active layer monitoring (calm) program:
368 Research designs and initial results, *Polar Geography*, 24, 166-258, 10.1080/10889370009377698, 2000.

369 Cao, B., Zhang, T., Wu, Q., Sheng, Y., Zhao, L., and Zou, D.: Permafrost zonation index map and
370 statistics over the Qinghai-Tibet Plateau based on field evidence, *Permafrost and Periglacial Processes*,
371 30, 178-194, 10.1002/ppp.2006, 2019.

372 Cao, B., Zhang, T., Peng, X., Mu, C., Wang, Q., Zheng, L., Wang, K., and Zhong, X.: Thermal
373 Characteristics and Recent Changes of Permafrost in the Upper Reaches of the Heihe River Basin,
374 Western China, *Journal of Geophysical Research: Atmospheres*, 123, 7935-7949,
375 <https://doi.org/10.1029/2018JD028442>, 2018.

376 Chen, S.-S., Zang, S., and Sun, L.: Characteristics of permafrost degradation in Northeast China and its
377 ecological effects: A review, *Sciences in Cold and Arid Regions*, 12, 1-11,
378 10.3724/sp.j.1226.2020.00001., 2020.

379 Douglas, T. A., Hiemstra, C. A., Anderson, J. E., Barbato, R. A., Bjella, K. L., Deeb, E. J., Gelvin, A. B.,
380 Nelsen, P. E., Newman, S. D., Saari, S. P., and Wagner, A. M.: Recent degradation of interior Alaska
381 permafrost mapped with ground surveys, geophysics, deep drilling, and repeat airborne lidar, *The
382 Cryosphere*, 15, 3555-3575, 10.5194/tc-15-3555-2021, 2021.

383 Everdingen, R. O. v.: Multi-language glossary of permafrost and related ground-ice terms, National Snow
384 and Ice Data Centre, Boulder, CO1998 (revised 2005).

385 Farquharson, L. M., Romanovsky, V. E., Cable, W. L., Walker, D. A., Kokelj, S. V., and Nicolsky, D.:
386 Climate Change Drives Widespread and Rapid Thermokarst Development in Very Cold Permafrost in
387 the Canadian High Arctic, *Geophysical Research Letters*, 46, 6681-6689,
388 <https://doi.org/10.1029/2019GL082187>, 2019.

389 Grebenets, V. I., Tolmanov, V. A., and Streletskiy, D. A.: Active Layer Dynamics Near Norilsk, Taimyr
390 Peninsula, Russia, *Geography, Environment, Sustainability*, 14, 55-66, 10.24057/2071-9388-2021-073,
391 2021.

392 Gruber, S.: Derivation and analysis of a high-resolution estimate of global permafrost zonation, *The*

393 Cryosphere, 6, 10.5194/tc-6-221-2012, 2012.

394 Guglielmin, M.: Ground surface temperature (GST), active layer and permafrost monitoring in
395 continental Antarctica, Permafrost and Periglacial Processes, 17, 133-143,
396 <https://doi.org/10.1002/ppp.553>, 2006.

397 Guglielmin, M., Worland, M. R., and Cannone, N.: Spatial and temporal variability of ground surface
398 temperature and active layer thickness at the margin of maritime Antarctica, Signy Island,
399 Geomorphology, 155-156, 20-33, <https://doi.org/10.1016/j.geomorph.2011.12.016>, 2012.

400 Guo, W., Liu, H., Anenkhonov, O. A., Shangguan, H., Sandanov, D. V., Korolyuk, A. Y., Hu, G., and Wu,
401 X.: Vegetation can strongly regulate permafrost degradation at its southern edge through changing
402 surface freeze-thaw processes, Agricultural and Forest Meteorology, 252, 10-17,
403 <https://doi.org/10.1016/j.agrformet.2018.01.010>, 2018.

404 He, R.-X., Jin, H.-J., Luo, D.-L., Li, X.-Y., Zhou, C.-F., Jia, N., Jin, X.-Y., Li, X.-Y., Che, T., Yang, X.,
405 Wang, L.-Z., Li, W.-H., Wei, C.-L., Chang, X.-L., and Yu, S.-P.: Permafrost changes in the Nanwenghe
406 Wetlands Reserve on the southern slope of the Da Xing'anling–Yile'huli mountains, Northeast China,
407 Advances in Climate Change Research, 12, 696-709, <https://doi.org/10.1016/j.accre.2021.06.007>, 2021.

408 Hrbáček, F., Vieira, G., Oliva, M., Balks, M., Guglielmin, M., de Pablo, M. Á., Molina, A., Ramos, M.,
409 Goyanes, G., Meiklejohn, I., Abramov, A., Demidov, N., Fedorov-Davydov, D., Lupachev, A., Rivkina,
410 E., Láska, K., Kňázková, M., Nývlt, D., Raffi, R., Strelin, J., Sone, T., Fukui, K., Dolgikh, A., Zazovskaya,
411 E., Mergelov, N., Osokin, N., and Miamin, V.: Active layer monitoring in Antarctica: an overview of
412 results from 2006 to 2015, Polar Geography, 44, 217-231, 10.1080/1088937X.2017.1420105, 2021.

413 Jin, H., Wu, Q., and Romanovsky, V.: Degrading permafrost and its impacts, Advances in Climate Change
414 Research, 12, 10.1016/j.accre.2021.01.007, 2021.

415 Jin, H., Li, S., Cheng, G., Shaoling, W., and Li, X.: Permafrost and climatic change in China, Global and
416 Planetary Change, 26, 387-404, [https://doi.org/10.1016/S0921-8181\(00\)00051-5](https://doi.org/10.1016/S0921-8181(00)00051-5), 2000.

417 Jin, H., Yu, Q., Lü, L., Guo, D., He, R., Yu, S.-p., Sun, G., and Li, Y.: Degradation of permafrost in the
418 Xing'anling Mountains, northeastern China, Permafrost and Periglacial Processes, 18, 245-258, 2007.

419 Li, X.-Y., Jin, H.-J., Wang, H.-W., Marchenko, S. S., Shan, W., Luo, D.-L., He, R.-X., Spektor, V., Huang,
420 Y.-D., Li, X.-Y., and Jia, N.: Influences of forest fires on the permafrost environment: A review, Advances
421 in Climate Change Research, 12, 48-65, <https://doi.org/10.1016/j.accre.2021.01.001>, 2021.

422 Li, X., Jin, H., He, R., Huang, Y., Wang, H., Luo, D., Jin, X., Lü, L., Wang, L., Li, W. h., Wei, C., Chang,
423 X., Yang, S., and Yu, S.: Effects of forest fires on the permafrost environment in the northern Da
424 Xing'anling (Hinggan) mountains, Northeast China, Permafrost and Periglacial Processes, 30, 163-177,
425 <https://doi.org/10.1002/ppp.2001>, 2019.

426 Luo, D., Guo, D., Jin, H., Yang, S., Phillips, M. K., and Frey, B.: Ecological Impacts of Degrading
427 permafrost, Frontiers in Earth Science, 10.3389/feart.2022.967530, 2022.

428 Luo, L., Ma, W., Zhuang, Y., Zhang, Y., Yi, S., Xu, J., Long, Y., Ma, D., and Zhang, Z.: The impacts of
429 climate change and human activities on alpine vegetation and permafrost in the Qinghai-Tibet
430 Engineering Corridor, Ecological Indicators, 93, 24-35, <https://doi.org/10.1016/j.ecolind.2018.04.067>,
431 2018.

432 Mu, C., Abbott, B. W., Norris, A. J., Mu, M., Fan, C., Chen, X., Jia, L., Yang, R., Zhang, T., Wang, K.,
433 Peng, X., Wu, Q., Guggenberger, G., and Wu, X.: The status and stability of permafrost carbon on the
434 Tibetan Plateau, Earth-Science Reviews, 211, 103433, <https://doi.org/10.1016/j.earscirev.2020.103433>,
435 2020.

436 Ran, Y., Li, X., and Cheng, G.: Climate warming over the past half century has led to thermal degradation

437 of permafrost on the Qinghai–Tibet Plateau, *The Cryosphere*, 12, 595–608, 10.5194/tc-12-595-2018,
438 2018.

439 Ran, Y., Li, X., Cheng, G., Che, J., Aalto, J., Karjalainen, O., Hjort, J., Luoto, M., Jin, H., Obu, J., Hori,
440 M., Yu, Q., and Chang, X.: New high-resolution estimates of the permafrost thermal state and
441 hydrothermal conditions over the Northern Hemisphere, *Earth Syst. Sci. Data*, 14, 865–884,
442 10.5194/essd-14-865-2022, 2022.

443 Romanovsky, V. E., Smith, S. L., and Christiansen, H. H.: Permafrost thermal state in the polar Northern
444 Hemisphere during the international polar year 2007–2009: a synthesis, *Permafrost and Periglacial*
445 *Processes*, 21, 106–116, <https://doi.org/10.1002/ppp.689>, 2010.

446 Schuur, E. A. G. and Mack, M. C.: Ecological Response to Permafrost Thaw and Consequences for Local
447 and Global Ecosystem Services, *Annual Review of Ecology, Evolution, and Systematics*, 49, 279–301,
448 10.1146/annurev-ecolsys-121415-032349, 2018.

449 Schuur, E. A. G., McGuire, A. D., Schädel, C., Grosse, G., Harden, J. W., Hayes, D. J., Hugelius, G.,
450 Koven, C. D., Kuhry, P., Lawrence, D. M., Natali, S. M., Olefeldt, D., Romanovsky, V. E., Schaefer, K.,
451 Turetsky, M. R., Treat, C. C., and Vonk, J. E.: Climate change and the permafrost carbon feedback, *Nature*,
452 520, 171–179, 10.1038/nature14338, 2015.

453 Serban, R., Serban, M., He, R., Jin, H., Yan, L., Xinyu, L., Wang, X., and Li, G.: 46-Year (1973–2019)
454 Permafrost Landscape Changes in the Holo Basin, Northeast China Using Machine Learning and Object-
455 Oriented Classification, *Remote Sensing*, 13, 1910, 10.3390/rs13101910, 2021.

456 Shiklomanov, N., Streletskiy, D., and Nelson, F.: Northern Hemisphere Component of the Global
457 Circumpolar Active Layer Monitoring (CALM) Program, 2012.

458 Shur, Y. and Jorgenson, M.: Patterns of Permafrost Formation and Degradation in Relation to Climate
459 and Ecosystems, *Permafrost and Periglacial Processes*, 18, 7–19, 10.1002/ppp.582, 2007.

460 Sim, T. G., Swindles, G. T., Morris, P. J., Baird, A. J., Cooper, C. L., Gallego-Sala, A. V., Charman, D.
461 J., Roland, T. P., Borken, W., Mullan, D. J., Aquino-López, M. A., and Gałka, M.: Divergent responses
462 of permafrost peatlands to recent climate change, *Environmental Research Letters*, 16, 034001,
463 10.1088/1748-9326/abe00b, 2021.

464 Smith, S. L., Romanovsky, V. E., Lewkowicz, A. G., Burn, C. R., Allard, M., Clow, G. D., Yoshikawa,
465 K., and Throop, J.: Thermal state of permafrost in North America: a contribution to the international
466 polar year, *Permafrost and Periglacial Processes*, 21, 117–135, <https://doi.org/10.1002/ppp.690>, 2010.

467 Wei, Z., Jin, H., Zhang, J., Yu, S., Han, X., Ji, Y., He, R., and Chang, X.: Prediction of permafrost changes
468 in Northeastern China under a changing climate, *Science China Earth Sciences*, 54, 924–935,
469 10.1007/s11430-010-4109-6, 2011.

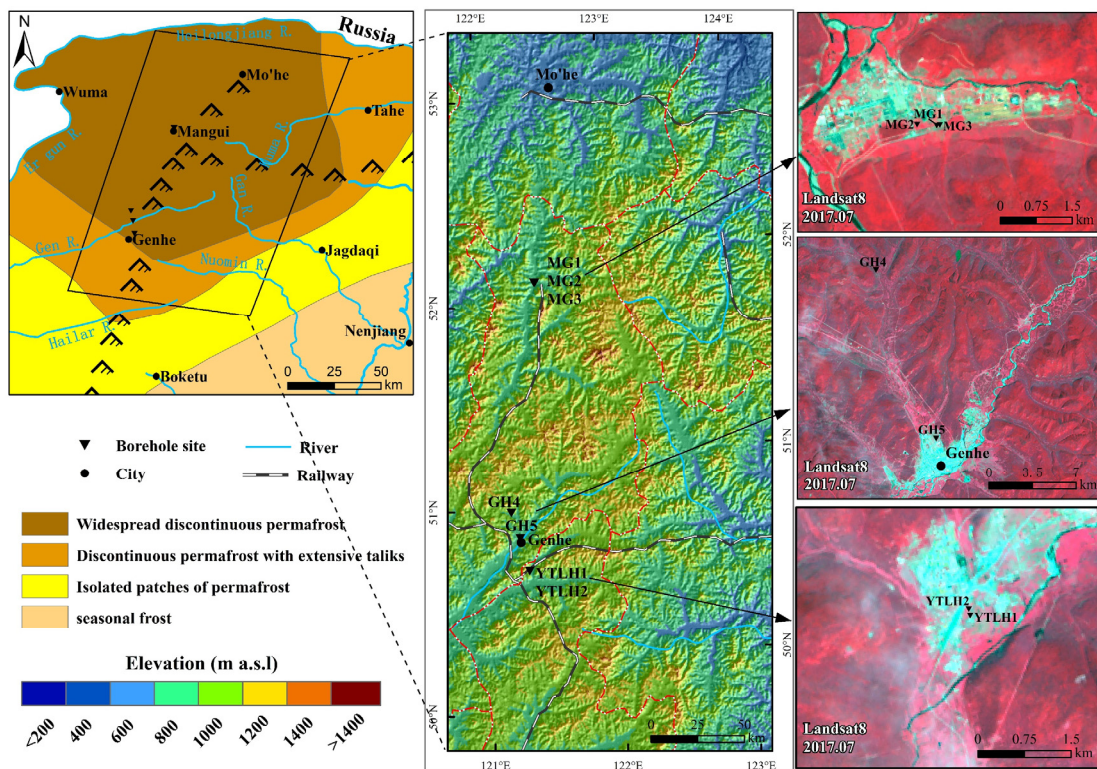
470 Wu, T., Xie, C., Zhu, X., Chen, J., Wang, W., Li, R., Wen, A., Wang, D., Lou, P., Shang, C., La, Y., Wei,
471 X., Ma, X., Qiao, Y., Wu, X., Pang, Q., and Hu, G.: Permafrost, active layer, and meteorological data
472 (2010–2020) at the Mahan Mountain relict permafrost site of northeastern Qinghai–Tibet Plateau, *Earth*
473 *Syst. Sci. Data*, 14, 1257–1269, 10.5194/essd-14-1257-2022, 2022.

474 Yang, J. M.: *Genhe annals (1996–2005)*, Inner Mongolia Culture Press, Hailar, 2007.

475 Yang, S. and Jin, H.: $\delta^{18}\text{O}$ and δD records of inactive ice wedge in Yitulihe, Northeastern China and
476 their paleoclimatic implications, *Science China Earth Sciences*, 54, 119–126, 10.1007/s11430-010-4029-
477 5, 2011.

478 Zhang, G., Nan, Z., Wu, X., Ji, H., and Zhao, S.: The Role of Winter Warming in Permafrost Change
479 Over the Qinghai-Tibet Plateau, *Geophysical Research Letters*, 46, 11261–11269,
480 <https://doi.org/10.1029/2019GL084292>, 2019.

481 Zhang, T., Nelson, F., and Gruber, S.: Introduction to special section: Permafrost and Seasonally Frozen
 482 Ground Under a Changing Climate, *Journal of Geophysical Research*, 112, 10.1029/2007JF000821, 2007.
 483 Zhang, Y., Cheng, G., Jin, H., Yang, D., Flerchinger, G., Chang, X., Wang, X., and Liang, J.: Influences
 484 of Topographic Shadows on the Thermal and Hydrological Processes in a Cold Region Mountainous
 485 Watershed in Northwest China, *Journal of Advances in Modeling Earth Systems*, 10,
 486 10.1029/2017MS001264, 2018a.
 487 Zhang, Y., Cheng, G., Jin, H., Yang, D., Flerchinger, G., Chang, X., Bense, V., Han, X., and Liang, J.:
 488 Influences of frozen ground and climate change on the hydrological processes in an alpine watershed: A
 489 case study in the upstream area of the Hei'he River, Northwest China, *Permafrost and Periglacial*
 490 *Processes*, 28, 420-432, 2017.
 491 Zhang, Z.-Q., Wu, Q.-B., Hou, M.-T., Tai, B.-W., and An, Y.-K.: Permafrost change in Northeast China
 492 in the 1950s–2010s, *Advances in Climate Change Research*, 12, 18-28,
 493 <https://doi.org/10.1016/j.accr.2021.01.006>, 2021.
 494 Zhang, Z., Wu, Q., Xun, X., Wang, B., and Wang, X.: Climate change and the distribution of frozen soil
 495 in 1980–2010 in northern northeast China, *Quaternary International*, 467, 230-241,
 496 <https://doi.org/10.1016/j.quaint.2018.01.015>, 2018b.
 497 Zhao, L., Zou, D., Hu, G., Wu, T., Du, E., Liu, G., Xiao, Y., Li, R., Pang, Q., Qiao, Y., Wu, X., Sun, Z.,
 498 Xing, Z., Sheng, Y., Zhao, Y., Shi, J., Xie, C., Wang, L., Wang, C., and Cheng, G.: A synthesis dataset of
 499 permafrost thermal state for the Qinghai–Tibet (Xizang) Plateau, China, *Earth Syst. Sci. Data*, 13, 4207-
 500 4218, 10.5194/essd-13-4207-2021, 2021.
 501 Zou, D., Zhao, L., Sheng, Y., Chen, J., Hu, G., Wu, T., Wu, J., Xie, C., Wu, X., Pang, Q., Wang, W., Du,
 502 E., Li, W., Liu, G., Li, J., Qin, Y., Qiao, Y., Wang, Z., Shi, J., and Cheng, G.: A new map of permafrost
 503 distribution on the Tibetan Plateau, *The Cryosphere*, 11, 2527-2542, 10.5194/tc-11-2527-2017, 2017.
 504



505

506 **Figure 1. Location of the study area and the distribution of Mangui1 (MG1), Mangui2 (MG2), Mangui3**
507 **(MG3), Gen'he4 (GH4), Gen'he5 (GH5), Yituli'he1 (YTLH1) and Yituli'he2 (YTLH2) in the zones of frozen**
508 **ground in the northern Da Xing'anling Mountains, Northeast China (The permafrost distribution is from Jin**
509 **et al. (2007).)**
510

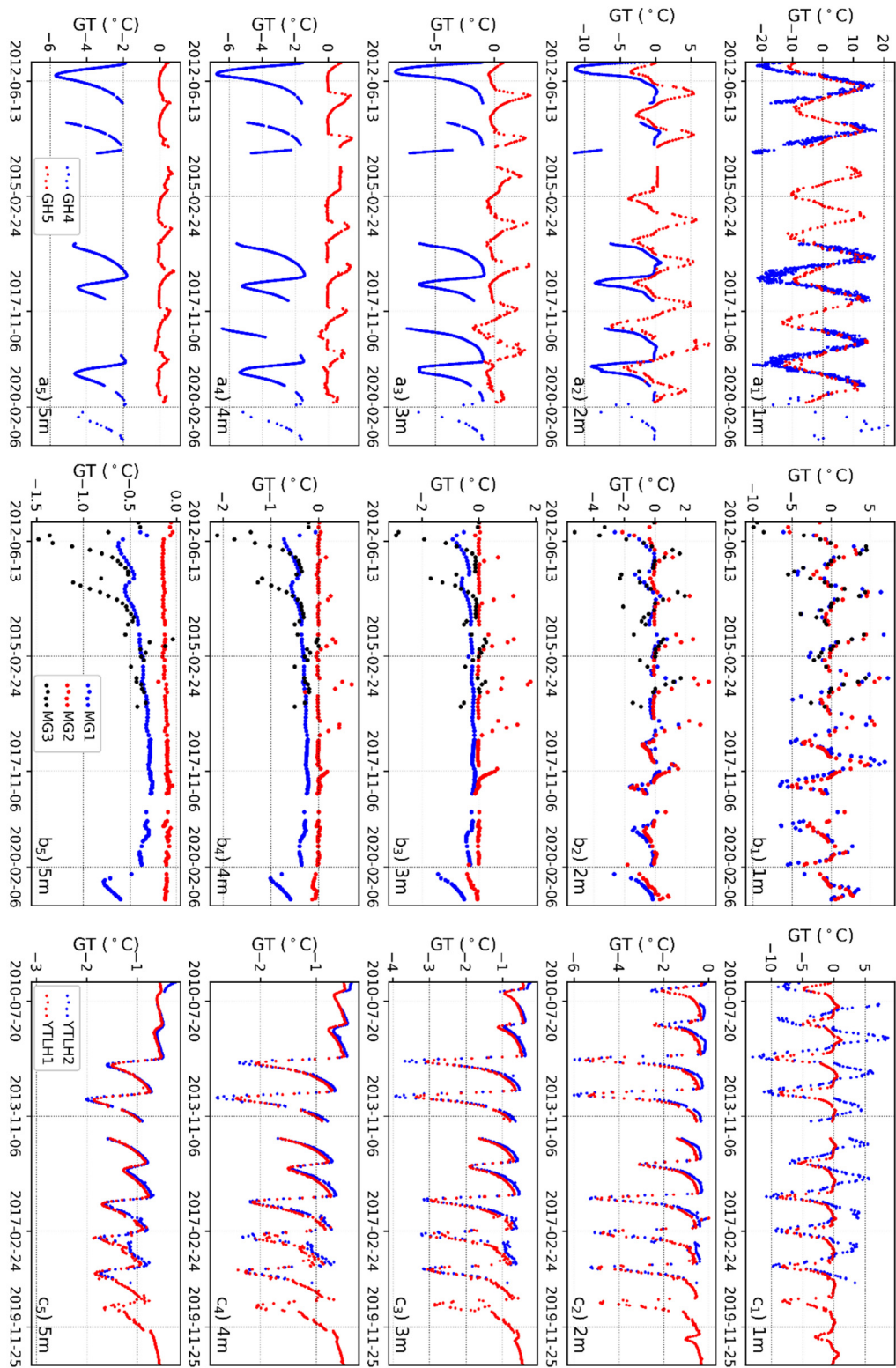


Figure 2. Variability of measured ground temperatures at depths of 1-5 m for Boreholes GH4 and GH5 (a), MG1, MG2 and MG3 (b), and YTLH1 and YTLH2 (c).

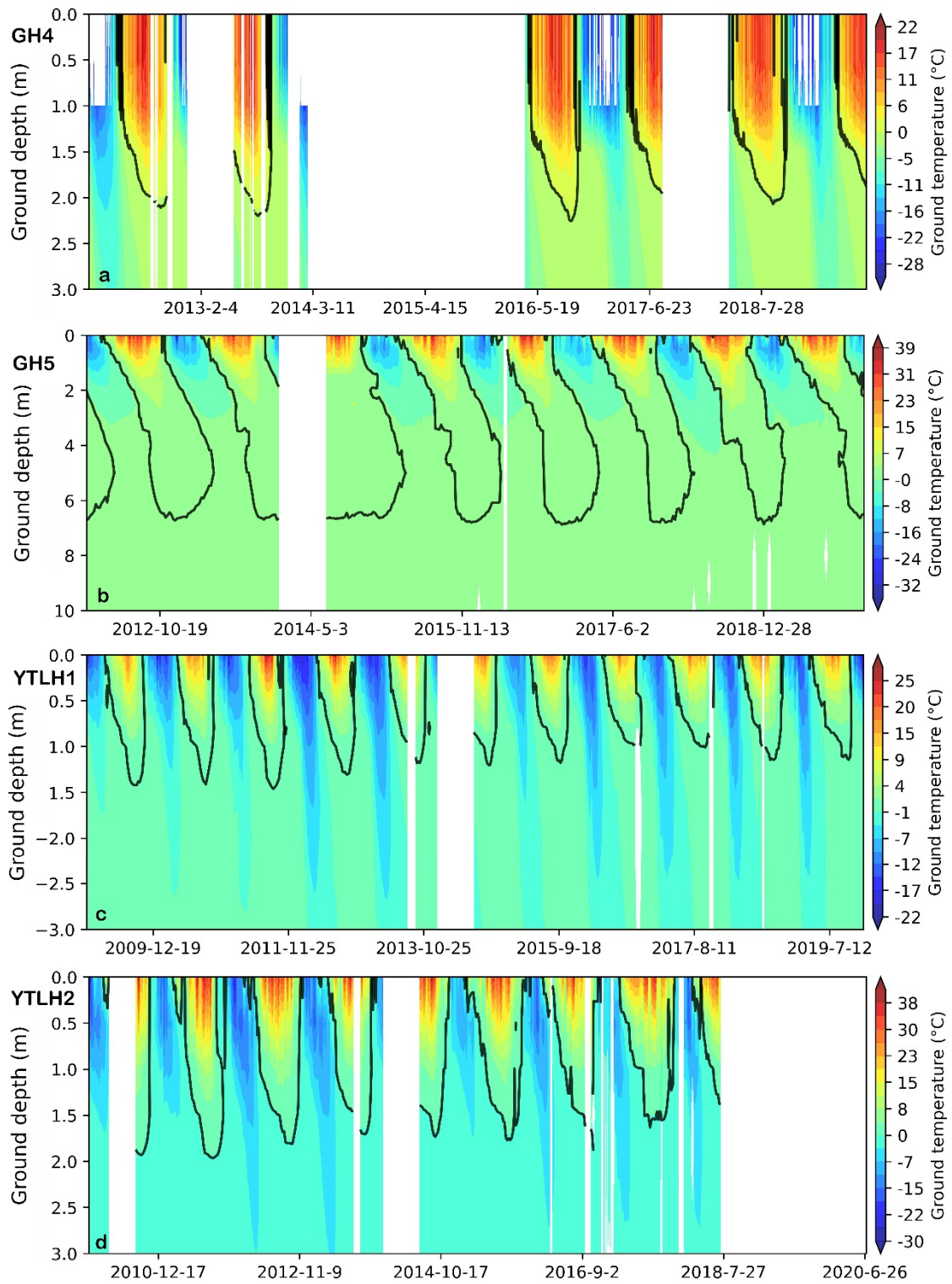


Figure 3 Variability of 0 °C isotherms (black curves) of ground temperature for Boreholes GH4 (a), GH5 (b), YTLH1 (c), and YTLH2 (d). The empty space indicates the period of missing data.

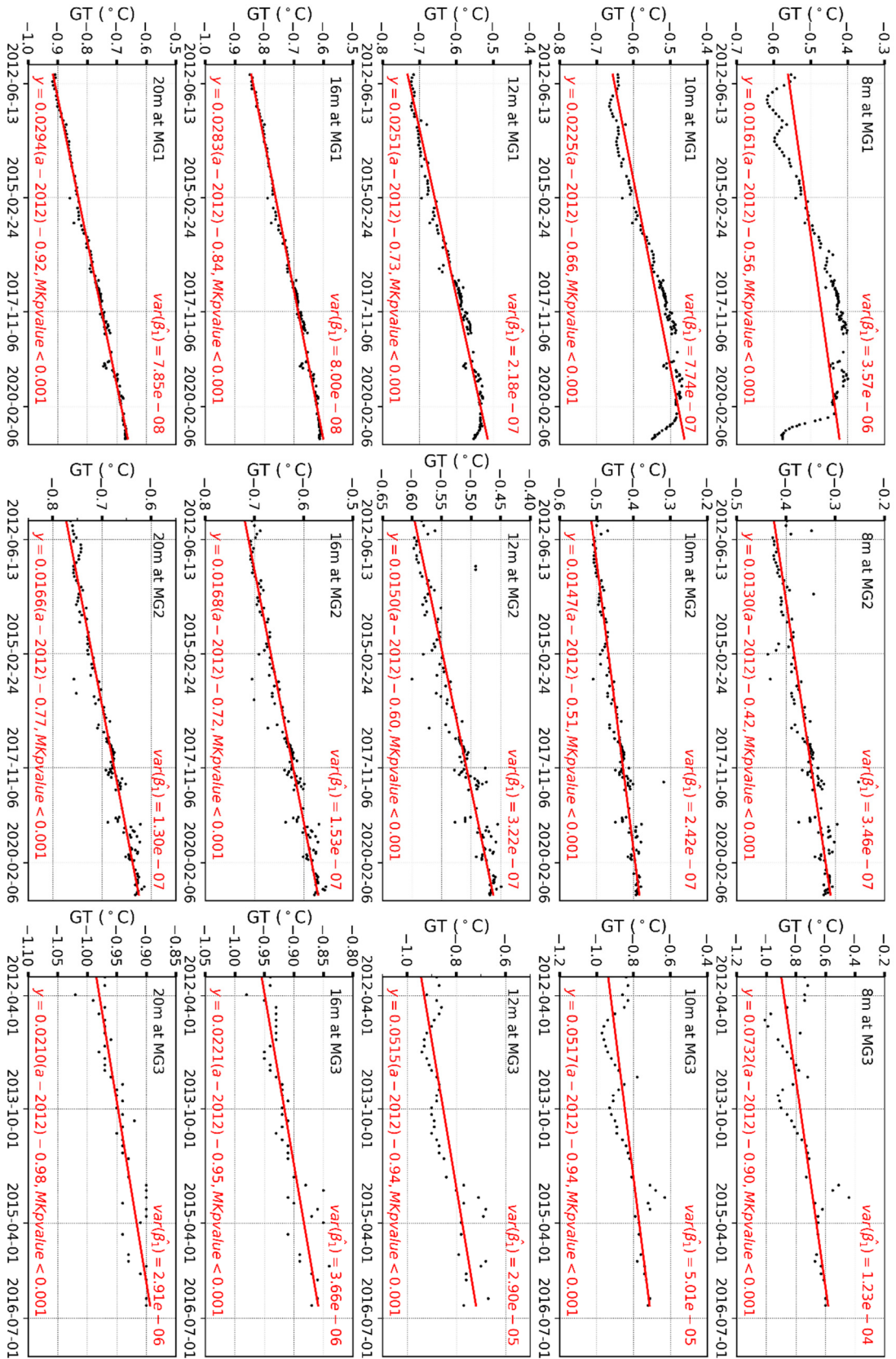


Figure 4. Variability of permafrost temperatures at depths of 8, 10, 12, 16 and 20 m in Boreholes MG1, MG2 and MG3 in Mangui, northern Da Xing'anling Mountains, Northeast China during 2012-2020. GT stands for ground temperature.

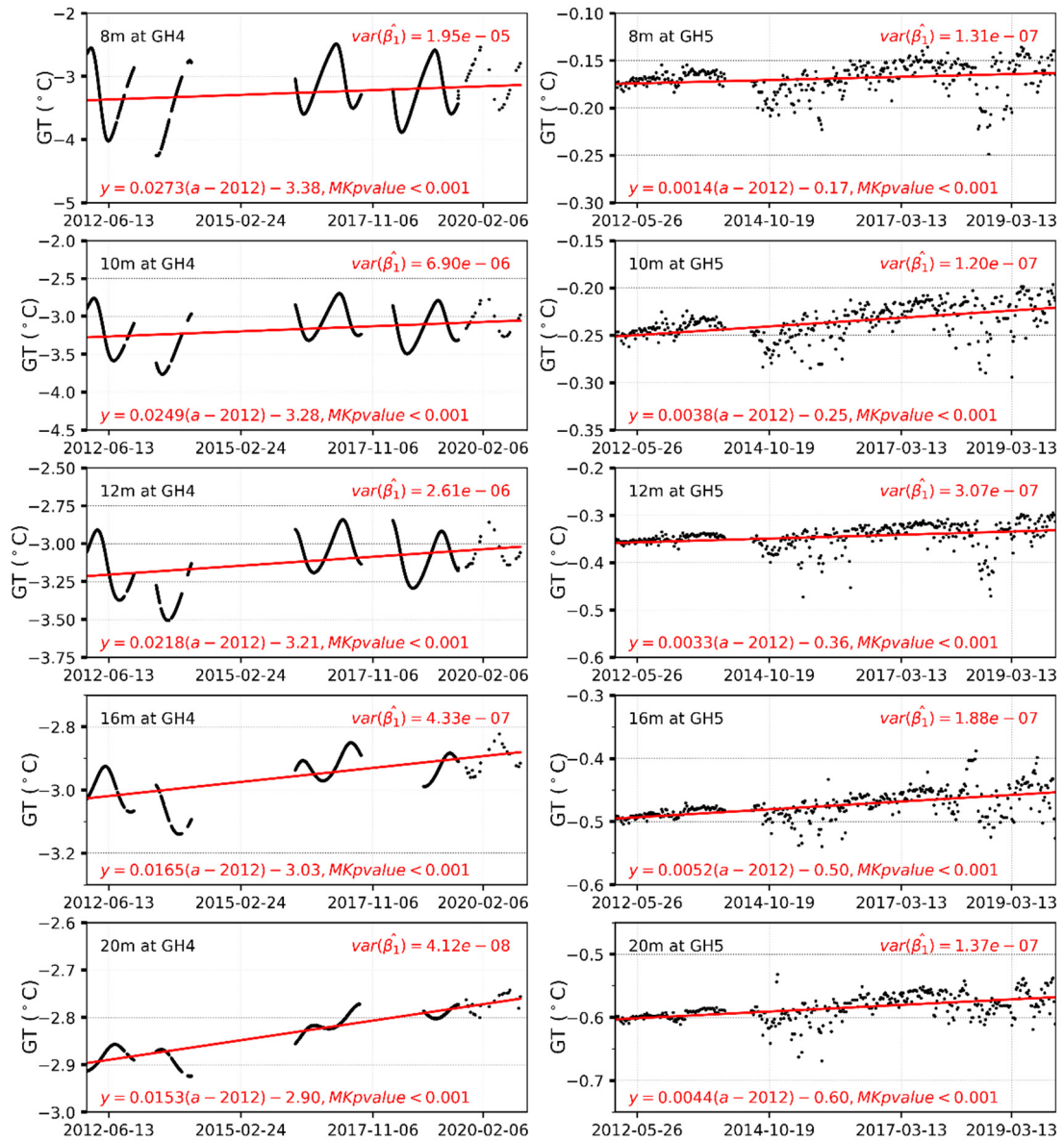


Figure 5. Variations in permafrost temperatures at depths of 8, 10, 12, 16 and 20 m in Boreholes GH4 and GH5 in Gen'he, northern Da Xing'anling Mountains, Northeast China during 2012-2020. GT stands for ground temperature.

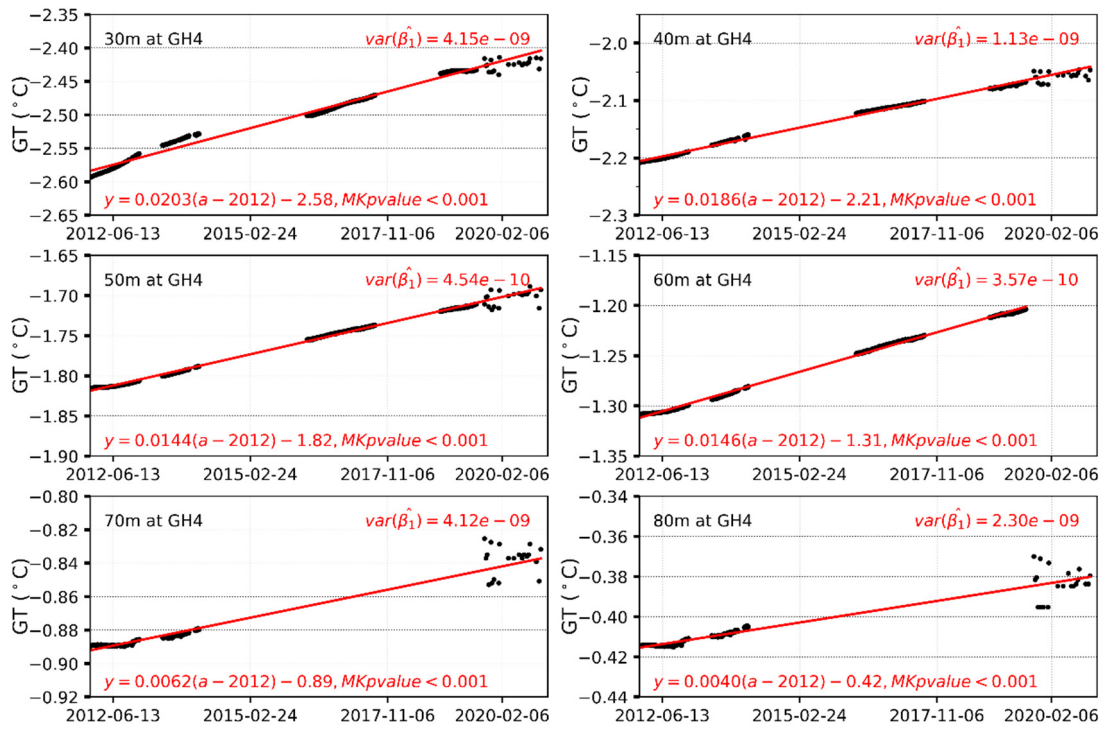


Figure 6. Variability of deep permafrost temperatures at depths of 30 – 80 m for Borehole GH4 in Gen’he, northern Da Xing’anling Mountains, Northeast China during 2012-2020. GT stands for ground temperature.

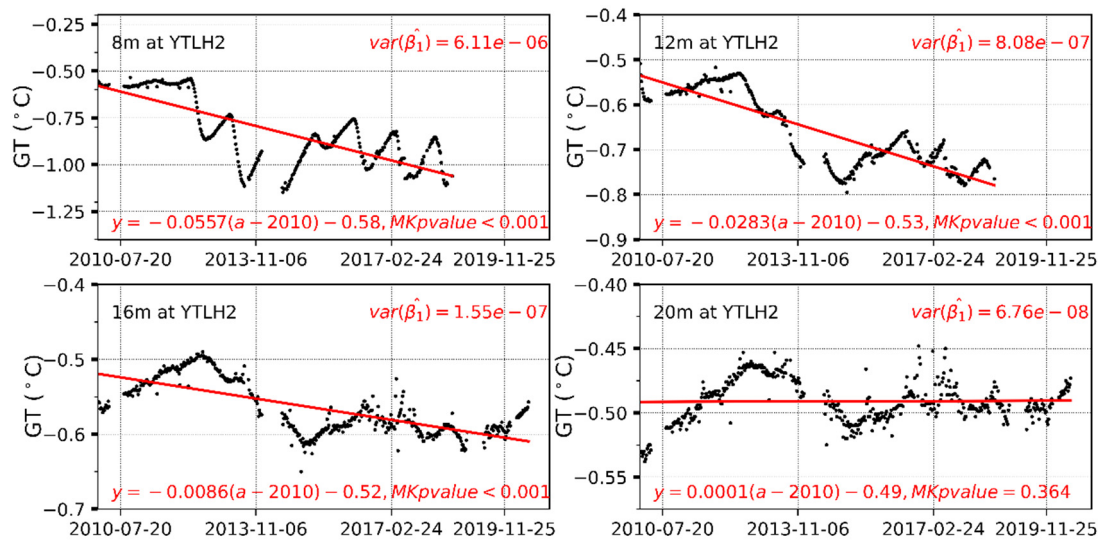


Figure 7. Variability of permafrost temperatures at depths of 8, 12, 16 and 20 m at Borehole YTLH2 in Yituli’he in northern Da Xing’anling Mountains, Northeast China during 2012-2020. GT stands for ground temperature.

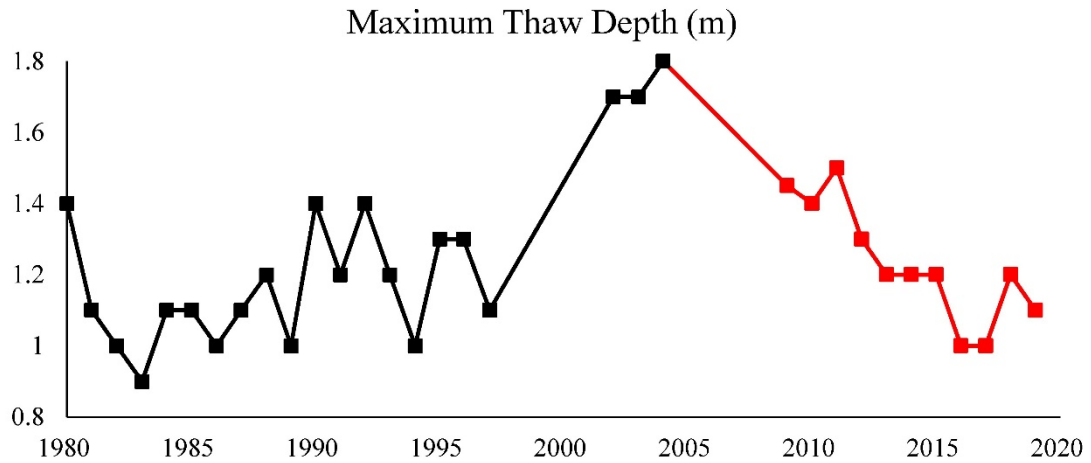


Figure 8. The maximum thaw depth (1980-2019) in Yituli'he on the northwestern flank of the northern Da Xing'anling Mountains in Northeast China (Black squares appeared in the paper from Jin et al. (2007), red ones are obtained in this observation. The two boreholes are 10 m from each other, with similar surface, hydrology and soil conditions.)

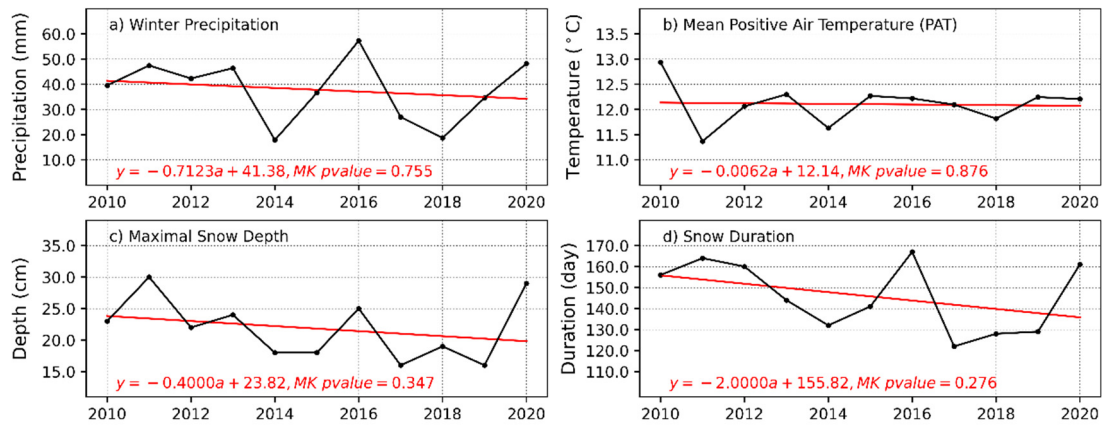


Figure 9. Climatic characteristics of Gen'he on the northwestern flank of the northern Da Xing'anling Mountains in Northeast China in the past ten years

Table 1. Characteristics and monitoring information of ground temperature boreholes in the northwestern part of Da Xing'anling Mountains, Northeastern China

Borehole No.	Lat. (°N)	Long. (°E)	Elev. (m a. s. l.)	Vegetation	Monitoring depths (m)	Time period	Monitoring frequency
MG1	52.037	122.069	633	<i>Betula</i>	0.0, 1.0, 1.5, 2.0, 2.5, 3.0, 3.5, 4.0, 4.5,	2012-2020	Monthly
				<i>fruticosa</i>			
MG2	52.036	122.075	642	shrubs	5.0, 6.0, 7.0, 8.0, 9.0, 10.0, 11, 12, 13, 14,	2012-2020	Monthly
				<i>Carex tato</i>			
MG3	52.036	122.076	639	meadow	15, 16, 17, 18, 19, 20	2012-2015	Monthly
				Open courtyard			
GH4	50.932	121.502	811	<i>Betula</i>	0.0, 1.0, 1.5, 2.0, 2.5, 3.0, 3.5, 4.0, 4.5,	2012-2014, 2016-2017,	Hourly
				<i>fruticosa</i>			
GH5	50.799	121.530	728	<i>Larix gmelini</i>	15, 16, 17, 18, 19, 20, 25, 30, 35, 40, 45,	2019-2020	Hourly
				forest			
YTLH1	50.629	121.549	721	50, 60, 70, 80	0.0, 1.0, 1.5, 2.0, 2.5, 3.0, 3.5, 4.0, 4.5,	2012-2019	Weekly
				<i>Carex tato</i>			
YTLH2	50.630	121.549	725	meadow	5.0, 6.0, 7.0, 8.0, 9.0, 10.0, 11, 12, 13, 14,	2010-2017	Weekly
				<i>Carex tato</i>			
YTLH2	50.630	121.549	725	swamp	15, 16, 17, 18, 19, 20	2010-2017	Weekly
				<i>Carex tato</i>			
YTLH2	50.630	121.549	725	swamp	15, 16, 17, 18, 19, 20	2010-2017	Weekly
				<i>Carex tato</i>			

Table 2 ALT and average MAGTs of boreholes at larger depths in the northwestern Da Xing'anling Mountains, Northeast China

Borehole	ALT (m)	Average MAGT (°C)				
		8m	10m	13m	16m	20m
MG1	1.9-2.6	-0.48(ZAA)	-0.55	-0.63	-0.71	-0.77
MG2	4.3-4.8	-0.34(ZAA)	-0.44	-0.55	-0.63	-0.69
MG3	2.8-4.0	-0.75	-0.83	-0.87(ZAA)	-0.91	-0.94
GH4	2.0-2.2	-3.26	-3.17	-3.06	-2.96(ZAA)	-2.84
GH5	7.0	-0.17(ZAA)	-0.24	-0.39	-0.47	-0.59
YTLH2	1.5-2.0	-0.82	-0.74	-0.61(ZAA)	-0.56	-0.49